Influence of Dynamic Properties and Position of Rivulet on Rain–Wind-Induced Vibration of Stay Cables

Wen-Li Chen[1]; Shan-Ran Tang[2]; Hui Li, M.ASCE[3]; and Hui Hu[4]

Abstract: This paper combines an experimental study and computational fluid dynamics (CFD) simulations to investigate the influence of dynamic properties and position of upper rivulet on rain–wind-induced vibration (RWIV) of stay cables. The reproduction of the RWIV of a stay cable model is first performed based on artificial rainfall wind tunnel tests with an ultrasonic transmission thickness measurement system, which can obtain the characteristics of rivulets on the surface of the stay cable model. On the basis of the test results, CFD simulations are then used to study the aerodynamic influence of an upper rivulet using two different CFD models: a vibrating cable model with a moving upper rivulet and a vibrating cable model with a fixed upper rivulet. CFD simulations suggest that the existence of the upper rivulet do not sufficiently to excite RWIV. It is confirmed that, when an upper rivulet oscillates in a specific range at the same frequency of a cable, it can significantly vary the aerodynamic force acting on the cable with the same frequency of the cable and the aerodynamic resonant excitation will lead to the occurrence of RWIV. **DOI: 10.1061/(ASCE)BE.1943-5592.0000443.** © *2013 American Society of Civil Engineers.*

CE Database subject headings: Cable-stayed bridges; Vibration; Computational fluid dynamics technique; Wind loads.

Author keywords: Stay cable; Upper rivulet; Rain–wind-induced vibration; Ultrasonic transmission thickness measurement system; Computational fluid dynamics.

Introduction

Rain–wind-induced vibration (RWIV) is a large-amplitude vibration and often occurs when rain and wind act simultaneously on stay cables. Hikami and Shiraishi (1988) first reported the RWIV phenomenon for stay cables in the Meiko Nishi bridge, and it was then observed in many other bridges. Many studies have been conducted over the last two decades through the use of field measurements (Hikami and Shiraishi 1988; Persoon and Noorlander 1999; Main and Jones 1999; Matsumoto et al. 2003a; Ni et al. 2007; Phelan et al. 2006; Zuo et al. 2008; Zuo and Jones 2010), wind tunnel tests (Hikami and Shiraishi 1988; Matsumoto et al. 1990, 1992, 1995, 1998, 2003b; Flamand 1995; Bosdogianni and Olivari 1996; Verwiebe and Ruscheweyh 1998; Gu and Du 2005; Cosentino et al. 2003; Li et al. 2010a), and theoretical analyses (Yamaguchi 1990; Xu and Wang 2003; Wilde and Witkowski 2003; Seidel and Dinkler 2006; Peil and Nahrath 2003; van der Burgh et al. 2006). Study results indicate that the upper rivulet oscillation around the stay cable plays a key role when RWIV occurs.

Several possible mechanisms of RWIV were proposed during years of research. Early studies done by Yamaguchi (1990) and Bosdogianni and Olivari (1996) investigated and explained RWIV using galloping theory. Matsumoto et al. (2001) considered RWIV as a special vortex-induced vibration caused by the interactions between Karman vortex and axial vortex. Further studies (Matsumoto et al. 2003b; Zuo and Jones 2010) suggested that RWIV was a vortex-induced vibration at high reduced velocity caused by the vortex shedding that is different from the classical Karman vortex. On the other hand, Gu and Lu (2001) and Gu and Huang (2008) investigated the aerodynamic characteristics of the cylinder with an attachment and brought up the concept of unsteady zone of upper rivulet in which the presence of rivulet would dramatically affects the aerodynamic forces and causes aerodynamic instability. Nevertheless, the precise mechanism of RWIV remains unknown owing to the lack of quantitative measurements to quantify the upper rivulet oscillation.

Cosentino et al. (2003) presented an approach to obtain the information of an upper rivulet by arranging wire pins distributed over the region where the upper rivulet appeared. However, the wires may affect the movement of the upper rivulets on the cable surface. Therefore, the ultrasonic technique, which is a nonintrusive approach, is considered (Li and Serizawa 2004). Li et al. (2010a) used an ultrasonic transmission thickness measurement system (UTTMS) based on ultrasonic transmission technique to obtain information about the rivulet around the cables. A wind tunnel test of an inclined cable model incorporated with the UTTMS was conducted to measure the time-dependent characteristics of the water rivulets forming on the cable during RWIV.

In this paper, the dynamic characteristics of water rivulets, which are closely related to the RWIV phenomenon, are first investigated to obtain the equilibrium position, oscillation amplitude, and frequency of water rivulets through an artificial rainfall wind tunnel

[1]Associate Professor, School of Civil Engineering, Harbin Institute of Technology, Harbin 150090, China; presently, Visiting Scholar, Dept. of Aerospace Engineering, Iowa State Univ., Ames, IA 50011 (corresponding author). E-mail: cwl_80@hit.edu.cn

[2]Research Assistant, School of Civil Engineering, Harbin Institute of Technology, Harbin 150090, China.

[3]Professor, School of Civil Engineering, Harbin Institute of Technology, Harbin 150090, China.

[4]Professor, Dept. of Aerospace Engineering, Iowa State Univ., Ames, IA 50011.

Note. This manuscript was submitted on February 29, 2012; approved on September 25, 2012; published online on September 27, 2012. Discussion period open until March 1, 2014; separate discussions must be submitted for individual papers. This paper is part of the ***Journal of Bridge Engineering***, Vol. 18, No. 10, October 1, 2013. ©ASCE, ISSN 1084-0702/2013/10-1021–1031/$25.00.

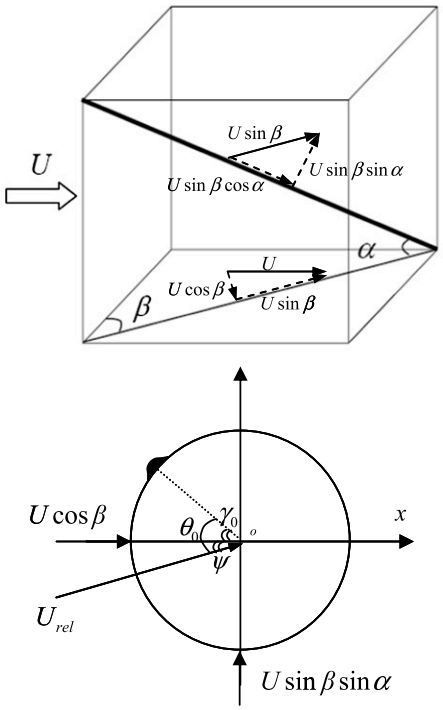

(a) Schematic diagram of the inclination angle

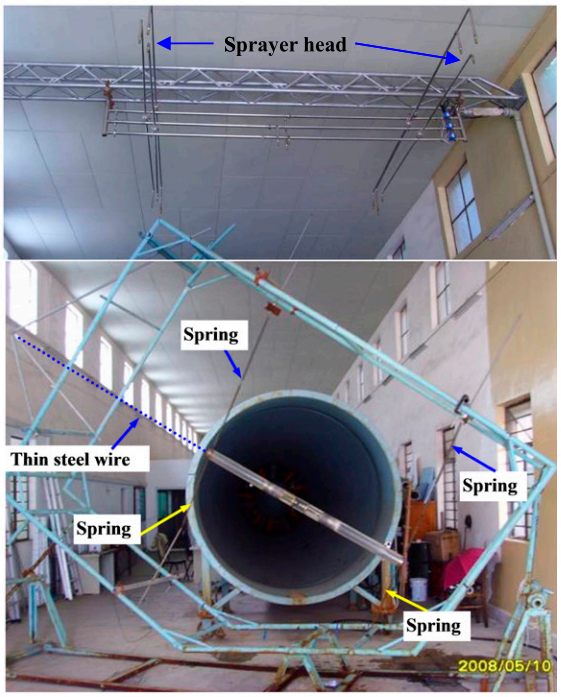

(b) Photograph of the testing setup for RWIV

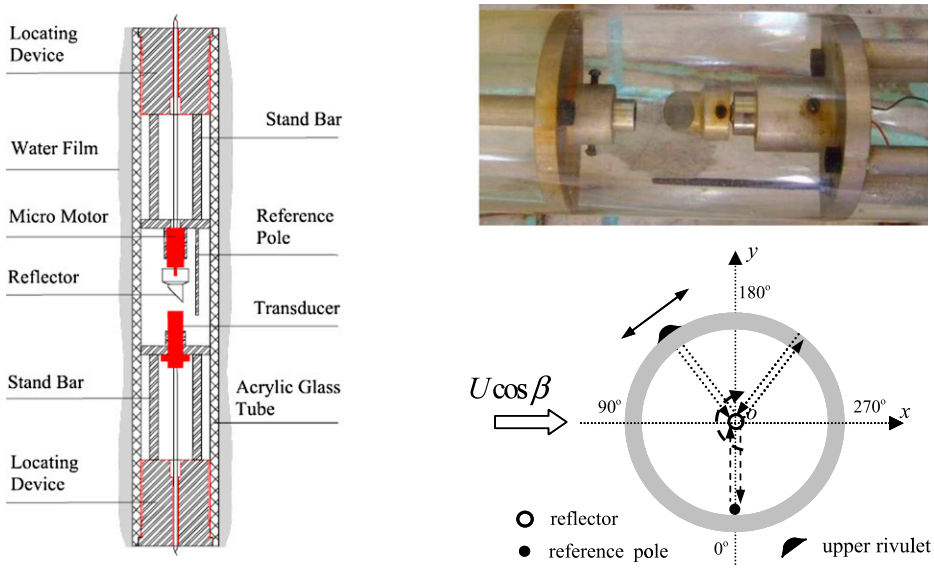

(c) Organization of the UTTMS

Fig. 1. Test measurement setup of the UTTMS: (a) schematic diagram of the inclination angle; (b) photograph of the testing setup for RWIV; (c) organization of the UTTMS (Li et al. 2010a, with permission from Elsevier)

test. On the basis of the characteristics of RWIV observed in the wind tunnel test with UTTMS, two types of computational fluid dynamics (CFD) models are established and computed. First, the CFD simulations of vibrating cable models with an oscillating upper rivulet are conducted to reproduce the RWIV phenomenon. Then, the simulations of the vibrating cable models with a fixed upper rivulet are performed to assess the effects of upper rivulet oscillation.

Wind Tunnel Tests of Rain–Wind-Induced Vibration with the Ultrasonic Transmission Thickness Measurement System and Results

Setup of Experiment

To reproduce the RWIV of the cable, a wind tunnel test is conducted in the TJ-1 atmospheric boundary layer wind tunnel, which

Table 1. Test Conditions for the RWIV of the Stay Cable

Condition	Result
Wind speed (m/s)	6–10
Reduced velocity	63–105
Reynolds number	$(3.8–6.4) \times 10^4$
Rainfall intensity (mm/h)	20–60
Inclination angle (degrees)	30
Yaw angle (degrees)	20–25

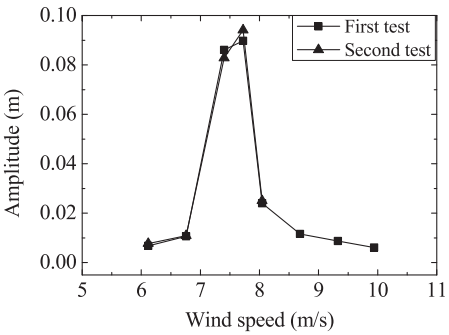

Fig. 2. Amplitude versus wind speed

is a straight-through wind tunnel with an original working section of 1.8 (width) × 1.8 m (height) located at Tongji University. An inclined stay cable model is used in this wind tunnel test. The inclination angles of the cable model α and the wind yaw angle β, as shown in Fig. 1(a), are two important parameters for RWIV and can be adjusted. The cross section of the inclined cable model is also shown in Fig. 1(a), where U is the wind velocity, the x-axis is the direction of the velocity component of $U\cos\beta$, the y-axis is the direction of the velocity component of $U\sin\beta\cos\alpha$ (cross-flow direction), U_{rel} is the relative wind velocity of the cable model, ψ is the wind attack angle between U_{rel} and the x-axis, γ_0 is the included angle between the equilibrium position of the upper rivulet and the x-axis, and θ_0 is the relative equilibrium angle between the equilibrium position of the upper rivulet and U_{rel}. The length is 2.0 m and the diameter is 0.1 m for the cable model with a mass of 17.15 kg. The natural vibration frequency is 0.952 Hz, and the cable damping ratio is 0.17%. Li et al. (2010a) investigated the experimental method using the UTTMS to obtain the characteristics of the vibration and the rivulet information of the stay cable model subject to RWIV. In this paper, we focus on the dynamic properties and position of rivulet, as well as their influence on RWIV. The test measurement setup for RWIV of the stay cable model with the UTTMS is shown in Figs. 1(b and c).

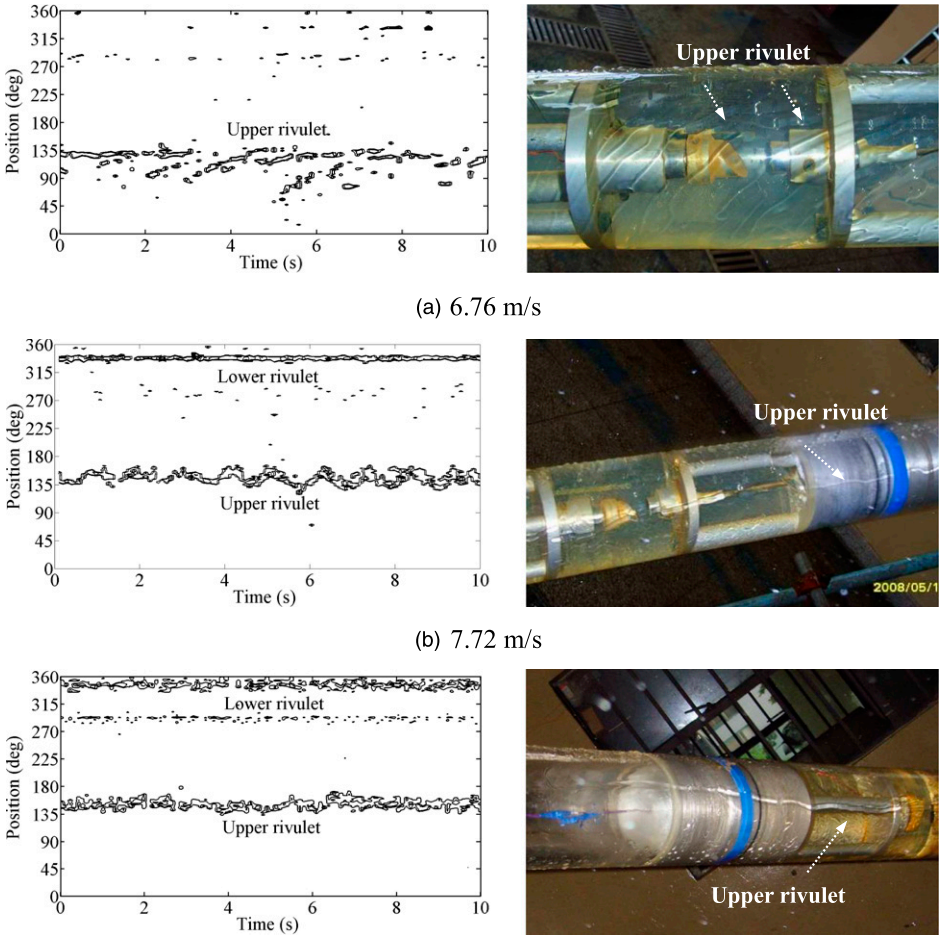

(a) 6.76 m/s

(b) 7.72 m/s

(c) 8.69 m/s

Fig. 3. Water rivulet contours along the circumferential direction measured by UTTMS and a corresponding snapshot of water rivulet distribution: (a) 6.76 m/s; (b) 7.72 m/s; (c) 8.69 m/s (Li et al. 2010b, with permission from Elsevier)

J. Bridge Eng., 2013, 18(10): 1021-1031

Dynamic Characteristics of Cable Vibration

The reduced velocity and Reynolds number are defined as U/fD and UD/ν, respectively, where U and ν are the wind speed and kinematic viscosity of the air, respectively. The test conditions for the RWIV of the cable are listed in Table 1. The diameter and the Reynolds number of the presented model in the wind tunnel are in the range of the prototype cables of the actual cable-stayed bridges.

According to a previous study (Gu and Du 2005), a rainfall intensity of 30 mm/h with an inclination angle of 30° for two test cases (yaw angles of 20 and 22.5° for the first and second tests, respectively) is used. Li et al. (2010b) studied the time history and frequency response of cable cross-flow displacement. The displacement amplitudes of the cable versus the wind velocity are shown in Fig. 2. It can be seen that RWIV occurs over the range of 6.76−8.04 m/s.

Dynamic Characteristics of Water Rivulets during Rain–Wind-Induced Vibration

The occurrence and duration of RWIV is closely associated with the formation, oscillation, and position of the upper rivulet. When a force balance condition meets, the rivulet could remain on the surface of the cable; otherwise, the rivulet may slide down from cable (low wind speed) or be blown away (high wind speed). Thus, the upper rivulet is observed only within a certain range of wind speeds. Figs. 3(a–c) present the water rivulets distribution on the surface measured by the UTTMS at wind speeds of 6.76, 7.72, and 8.69 m/s, respectively (Li et al. 2010b). As the wind speed continuously increases to 8.69 m/s, no RWIV is observed, yet the upper rivulet still remains; however, the steady circumferential oscillation of the upper rivulet gradually disappears as shown in Fig. 3(c).

The previous investigations consisting of field measurements and wind tunnel tests indicated that the equilibrium position and oscillation amplitude of upper rivulet would vary with wind speed. The UTTMS can capture the instantaneous position of the upper rivulet during oscillation and thereby obtain the equilibrium position, oscillation amplitude, and oscillation frequency. Fig. 4 shows the cross-flow amplitude of the cable model and the equilibrium position of the upper rivulet oscillation versus wind speed. When the wind speed is less than 7.40 m/s, the axially continuous upper rivulet does not form. Therefore, only the equilibrium positions under a range of 7.40−9.94 m/s are depicted in the figure. The equilibrium position or the static position is elevated with the increasing wind speed, regardless of the occurrence or not of the RWIV of the cable model.

According to the previous studies with cable models and artificial rivulets (Yamaguchi 1990; Gu and Lu 2001), the aerodynamic coefficients would change dramatically if the artificial rivulet is fixed within the positions of 50–70°. For the two tests of the current study, when the wind speed is within the range of 7.40−7.72 m/s, a continuous upper rivulet is found to form, and large-amplitude RWIV would occur. The equilibrium positions of the upper rivulet measured by UTTMS under RWIV are listed in Table 2. Referring to Fig. 1(a), the relative equilibrium angle θ_0 with a wind speed of 7.40−7.72 m/s is included in the range of 63–67°, which is consistent with the findings of the previous studies.

The cross-flow RWIV amplitude of the cable model and the RMS of the upper rivulet oscillation are plotted together in Fig. 5. It can be seen that the RMS of the upper rivulet oscillation is larger when RWIV occurs and then decreases dramatically accompanied by the disappearance of the RWIV of the stay cable when the wind speed is greater than 7.72 m/s. Such observation indicates that the cable vibration could excite the oscillation of the upper rivulet. The RMS of the upper rivulet oscillation for the four experimental points at wind speeds of 7.40 and 7.72 m/s is approximately 7°. Considering that θ_0 is in the range of 63–67°, the relative position angle θ is approximately in the range of 55–75° with an amplitude of approximately 10° when upper rivulet oscillates with RWIV in the wind tunnel tests.

The large amplitude of the upper rivulet oscillation is coupled with the dramatic cross-flow vibration of the cable model. The

Table 2. Equilibrium Positions of the Upper Rivulet under RWIV

Test	α (degrees)	β (degrees)	ψ (degrees)	γ_0 (degrees)	θ_0 (degrees)
First test	30	20	10.31	54.43–56.35	64.74–66.66
Second test	30	22.5	11.70	52.05–54.31	63.75–66.01

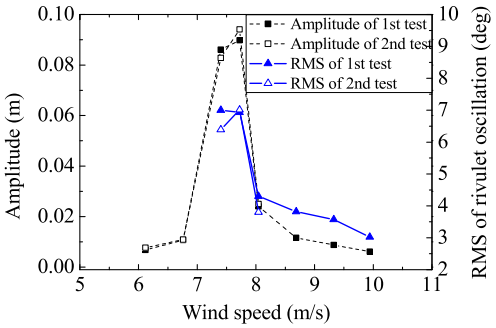

Fig. 5. RMS of upper rivulet oscillation and amplitude versus wind speed

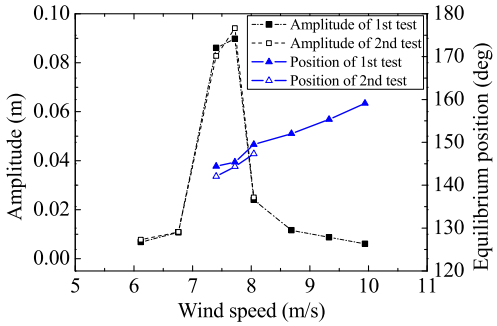

Fig. 4. Equilibrium position of upper rivulet and amplitude versus wind speed

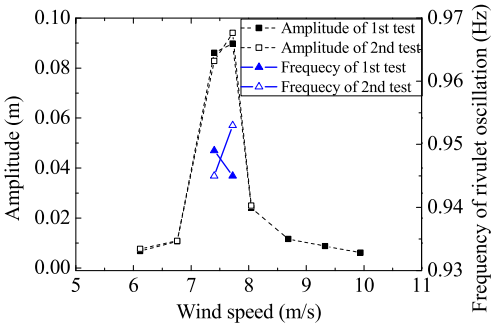

Fig. 6. Frequency of upper rivulet oscillation and amplitude versus wind speed

J. Bridge Eng., 2013, 18(10): 1021-1031

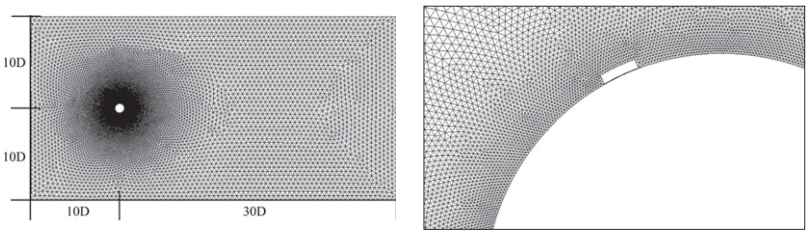

(a) Overall size of flow field (D=100mm)

(b) Fractionate gain around the upper rivulet

Fig. 7. Grid partition of the CFD simulation: (a) overall size of flow field ($D = 100$ mm); (b) fractionate gain around the upper rivulet

coupled strong vibration may be attributed to the relationship in the frequency of the rivulet and the cable model. The frequency response indicates that the dominant frequencies of the upper rivulet oscillation are 0.949 and 0.945 Hz at wind speeds of 7.40 and 7.72 m/s, respectively, for the first test, and 0.945 and 0.953 Hz for the second test, as shown in Fig. 6. These four frequencies are very close to 0.952 Hz, which is the natural frequency of the cable model. Outside the wind speed range of occurrence of the RWIV, the upper rivulet oscillation is random, as shown in Fig. 3(c), and there is no dominant frequency of the oscillation identified in spectral analysis.

According to this analysis, the upper rivulet oscillation has a relative equilibrium position between 63 and 67°, an amplitude of approximately 10°, and an oscillation frequency of approximately 0.952 Hz, which is the same with the cable vibration during RWIV at the test condition mentioned previously. These results will be used to determine the parameters of the upper rivulet in the CFD simulations.

Two-Dimensional Computational Fluid Dynamics Simulations of the Cable Model with Upper Rivulet

The results of the wind tunnel tests described previously indicate that the upper rivulet and its oscillation play important roles when RWIV occurs. A continuous upper rivulet would form along the cable only within a certain range of wind speed, and its existence is a necessary, but not a sufficient, condition for RWIV. The appearance of RWIV depends on the dynamic characteristics of the upper rivulet (Fig. 4) and also affects its circumferential oscillation amplitude and frequency (Figs. 5 and 6). The interaction between cable vibration and rivulet oscillation is the key to RWIV. In the current study, CFD simulation is used to investigate how the motion and position of the upper rivulet influence the cable vibration. To capture the essence of RWIV, a fundamental two-dimensional model is used. As a result, the axial flow and axial vortex are not considered in the current study. Moreover, the lower rivulet scarcely moves with or without the occurrence of RWIV and therefore is ignored in the CFD studies.

The shear stress transport (SST) $k - \omega$ turbulent model based on the Reynolds-averaged Navier-Stokes (RANS) method is used to simulate the turbulent behavior of the flow with CFD software *ANSYS FLUENT 12.1*. Fig. 7 shows the grid partition and size of the fluid field in the CFD study. The number of triangular cells is roughly 60,000, and the first grid normal to the cable surface is set as 0.5 mm. The boundary conditions are defined as follows: the left side is the velocity inlet, the right side is the pressure outlet, the upper and lower sides are symmetry, and the cable and the upper rivulet are considered as two separating wall surfaces. Because the Reynolds

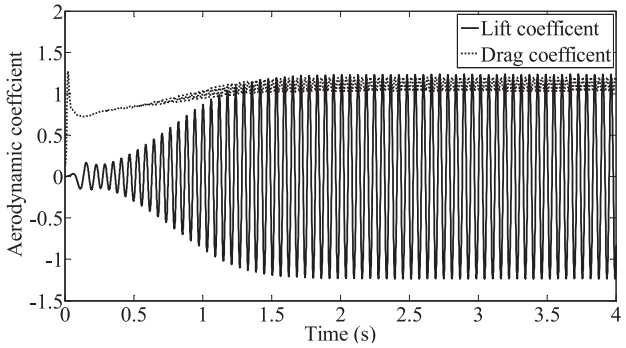

Fig. 8. Time histories of aerodynamic coefficients

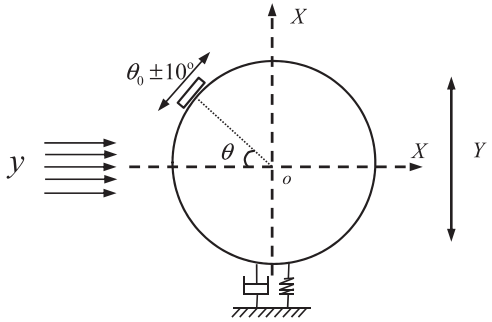

Fig. 9. Dynamic model of a vibrating cable with an upper rivulet

number (Table 1) is within the subcritical zone, the vortex shedding frequency of a cylinder can be estimated through the Strouhal number. When RWIV occurs, the expected vortex shedding period is approximately 0.06–0.07 s. Thus, the time step of 0.001 s is selected to provide enough sample points within one period of the RWIV.

A cable model without rivulet is calculated under the typical RWIV wind speed of 7.5 m/s to verify the CFD simulation setup. Fig. 8 shows the time histories of the aerodynamic coefficients. The average drag and fluctuating lift aerodynamic coefficient are 1.16 and 0.76, whereas their frequencies are 32.98 and 16.49 Hz, respectively. The corresponding Strouhal number S is 0.22. The averaged drag coefficient and Strouhal number are found to be very close to those reported in previous numerical and experimental studies (Elmiligui et al. 2004), with a similar Reynolds number (i.e., R = 50,000) as the present study. The fluctuating lift coefficient of the current study is found to be larger than the predicted value (i.e., 0.42) of the three-dimensional (3D) numerical simulation of Lu et al. (1997) at R = 44,200. Nevertheless, it is known that the

fluctuating lift coefficients of two-dimensional (2D) numerical simulations would be larger than those of 3D simulations in general. The quantitative comparison shows that the simulation results of the current study match the previous experimental and numerical results well.

One Degree-of-Freedom Cable Model with an Oscillating Upper Rivulet

To reproduce the RWIV of the cable with a CFD simulation, first a mechanical model of the cable is established, as shown in Fig. 9. The upper rivulet is given a preprogrammed harmonic oscillation expressed in Eq. (1) with the same frequency as that of the cable, according to the analysis described previously (Figs. 4–6). The cable is considered as a one degree-of-freedom (DOF) vibrating system under aerodynamic lift force, and its dynamic equation is given in Eq. (2)

$$\theta = a\sin(\omega t) + \theta_0, \quad a = 10^o \tag{1}$$

$$\ddot{y} + 2\xi\omega\dot{y} + \omega^2 y = \frac{0.5\rho D U_{rel}^2}{m_c} C_L(\theta) \tag{2}$$

where y = displacement of the cable in the cross-flow direction, θ = relative position angle of the upper rivulet, and θ_0 = relative equilibrium angle. In the equation, $\xi = 0.17\%$ is the cable damping ratio, and $\omega = 2\pi \times 0.952 = 5.98\,\text{rad/s}$ is the natural circular frequency. Furthermore, m_c is the mass per unit length of the tested cable section model, which equals 8.575 kg/m, and $D = 0.1$ m is the diameter of the cable. These parameters are the same as those for the cable model used in the wind tunnel test. ρ is the air density, and $C_L(\theta)$ is the aerodynamic lift coefficient automatically computed by the *ANSYS FLUENT 12.1* software, which is a function of angle θ.

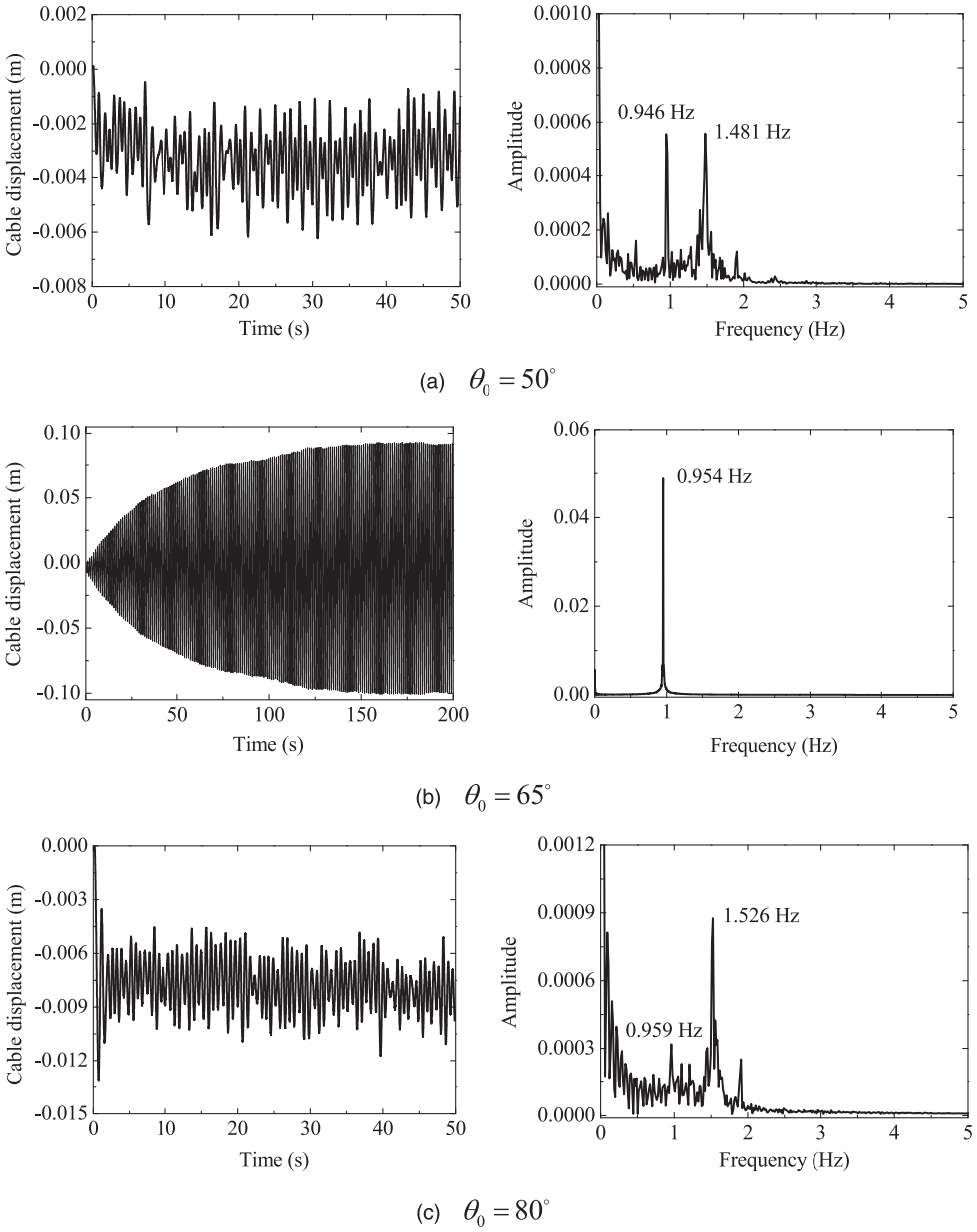

Fig. 10. Vibration response of the CFD cable model with an oscillating upper rivulet: (a) $\theta_0 = 50°$; (b) $\theta_0 = 65°$; (c) $\theta_0 = 80°$

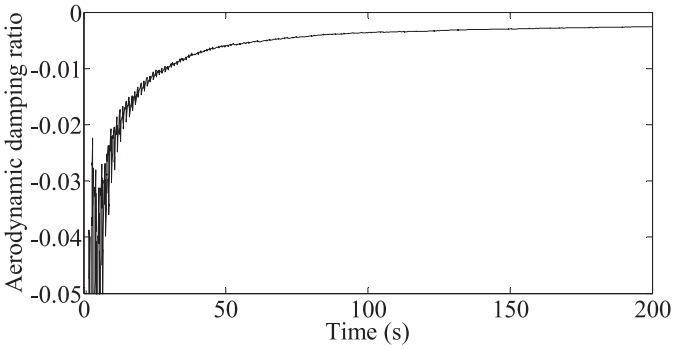

Fig. 11. Time history of equivalent aerodynamic damping ratio

From Fig. 1(a), U_{rel} can be calculated by taking $\alpha = 30°$, $\beta = 20°$, and $U = 7.5\,\mathrm{m/s}$, which is in the range where RWIV occurs.

$$U_{rel} = \sqrt{(U\sin\alpha\sin\beta)^2 + (U\cos\beta)^2} = 7.16\,\mathrm{m/s} \qquad (3)$$

Eq. (2) is solved by a user-defined function (UDF) based on the Newmark method to obtain the displacement that defines the locations of the cable and rivulet. Moreover, the UDF also defines the oscillation of the upper rivulet on the cable surface through Eq. (1). After computing the flow field in each time step, the UDF updates the positions of both the cable and rivulet. Then the dynamic mesh engages to remesh and smooth the grid cells for computing at the next time step.

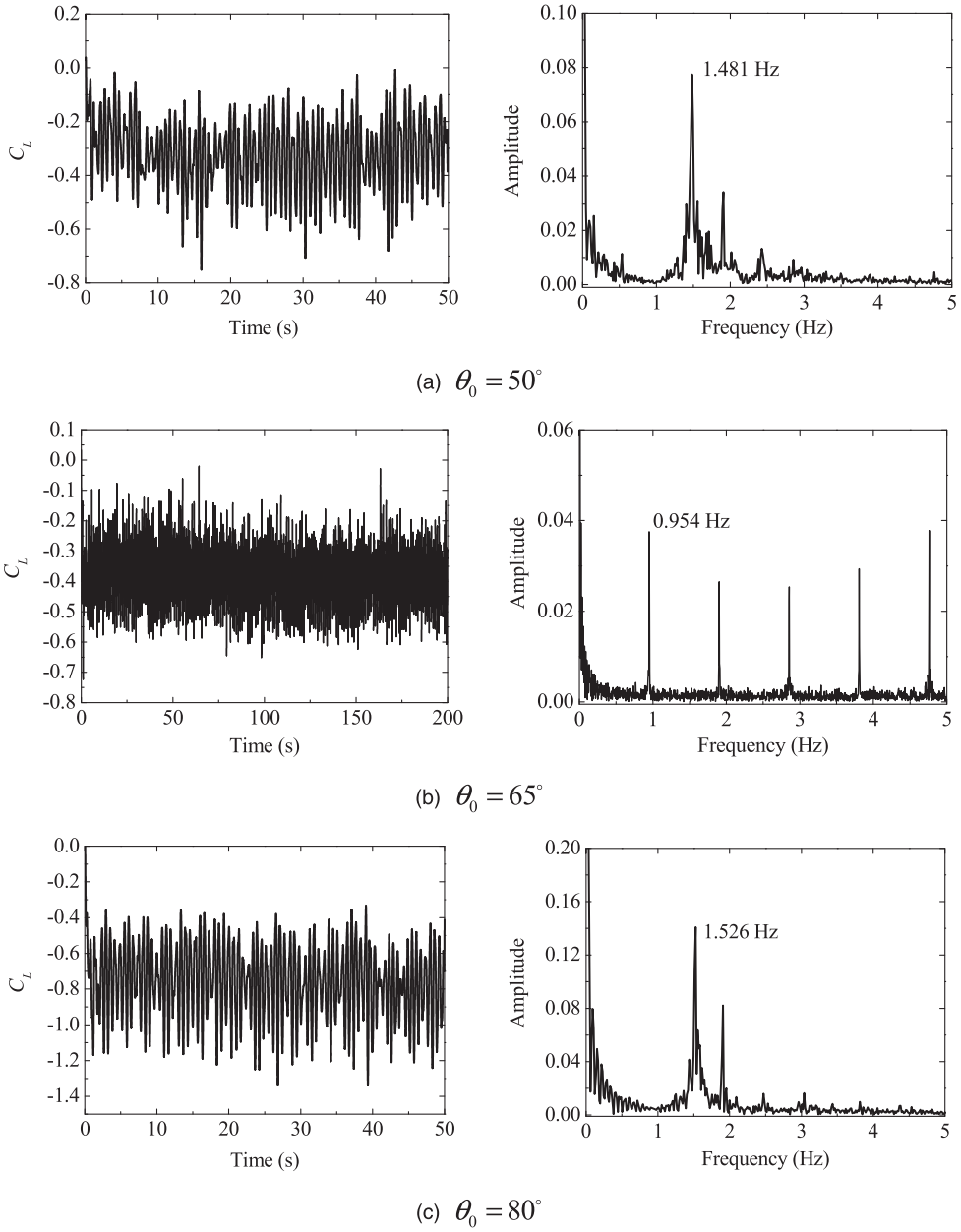

Fig. 12. Aerodynamic lift coefficients of the CFD cable model with an oscillating upper rivulet: (a) $\theta_0 = 50°$; (b) $\theta_0 = 65°$; (c) $\theta_0 = 80°$

J. Bridge Eng., 2013, 18(10): 1021-1031

The upper rivulet is represented by a rectangle with a height of 2 mm and a width of 8 mm in the CFD simulations [Fig. 7(b)]. The width of 8 mm is close to the measured rivulet width (Li et al. 2010a). The height used in the CFD model is about four times the measured rivulet height (~0.5 mm), which was determined mainly by the size of the first grid normal to the cable surface to ensure several grids in the direction of rivulet height. To choose the same height as the experimental measurement would demand a much smaller grid, which would dramatically increase the computation power requirement and also cause a negative volume problem during dynamic meshing. Additionally, the relative height of the rivulet (the ratio between rivulet height and cable diameter) in previous studies (Yamaguchi 1990; Gu and Lu 2001) is in the range of 0.03–0.2, which is much larger than 0.005 for the test results (Li et al. 2010a) but similar to 0.02 for the present CFD simulation.

Three different conditions are chosen to study how the cable vibration is affected by different ranges of the oscillations of the upper rivulet. The simulation results of the cases in which the relative equilibrium angle θ_0 equals 50, 65, and 80° are shown in Fig. 10. According to the experimental results shown in Table 2, the case $\theta_0 = 65°$ is in the range where the RWIV occurred and the other two cases are out of this range in the wind tunnel tests.

In Figs. 10(a and c), small vibrations with an amplitude less than 5 mm are observed. Moreover, the displacement histories of the cable seem very random. Compared with the large and systematic cable vibrations captured in the wind tunnel test (Li et al. 2010b), the CFD simulations indicate that RWIV does not occur when the relative equilibrium angle of the upper rivulet is 50 or 80°.

A systematic and regular vibration of the cable with a large amplitude is observed only when the upper rivulet oscillates in the

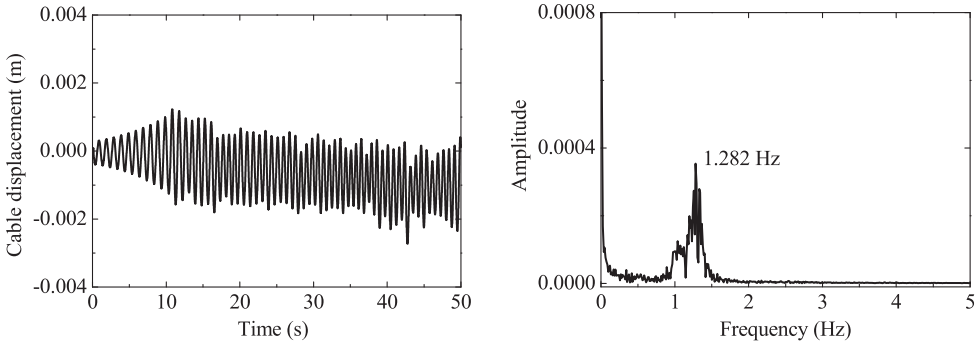

(a) $\theta_0 = 50^\circ$

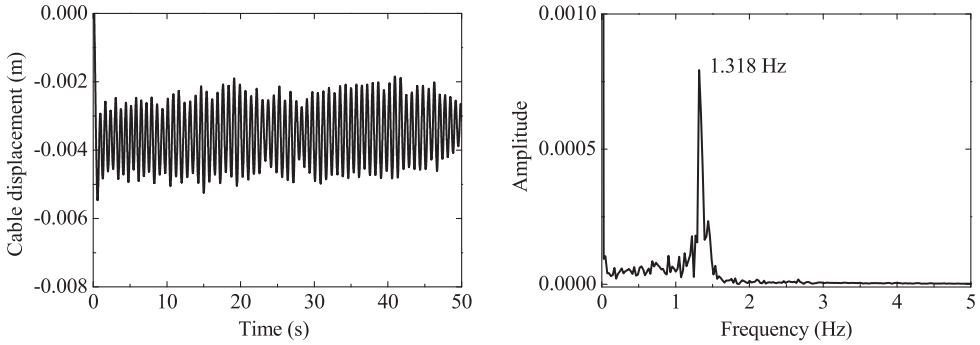

(b) $\theta_0 = 65^\circ$

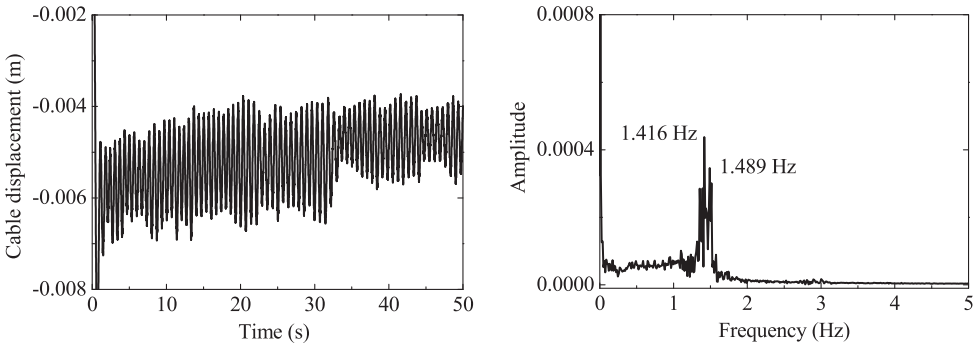

(c) $\theta_0 = 80^\circ$

Fig. 13. Displacement response of the CFD cable model with a fixed upper rivulet: (a) $\theta_0 = 50°$; (b) $\theta_0 = 65°$; (c) $\theta_0 = 80°$

range of 55–75° [Fig. 10(b)]. In this case, the amplitude increases to approximately 0.1 m when the vibration reaches its steady state, which agrees well with the observation in the wind tunnel test (Li et al. 2010b). Hence, RWIV is also successfully reproduced by this CFD simulation with an upper rivulet oscillating harmonically in the same region. In addition, the equivalent aerodynamic damping ratio is illustrated in Fig. 11. The aerodynamic damping is calculated by using an energy balance method, in which the equivalent viscous damping force is considered to have the same power as that of lift aerodynamic force in each vibration period. As shown in Fig. 11, the aerodynamic damping ratio keeps increasing with the development of RWIV until it approaches the negative value of the cable damping ratio.

The time histories and spectra of aerodynamic lift coefficients at the relative equilibrium angles of 50, 65, and 80° were analyzed and are shown in Figs. 12(a–c), respectively. The amplitudes of the lift coefficients are close, but the frequency components are different for the three cases. When the equilibrium angles are 50 and 80°, the dominant frequencies do not include the natural frequency of the cable. However, for the relative equilibrium angle of 65°, the dominant frequencies are multiple of the natural frequency, also including the natural frequency. It is the main reason that the RWIV of the cable can occur.

One Degree-of-Freedom Cable Model with a Fixed Upper Rivulet

Second, similar CFD simulations are conducted using nearly the same setup used in "One Degree-of-Freedom Cable Model with an

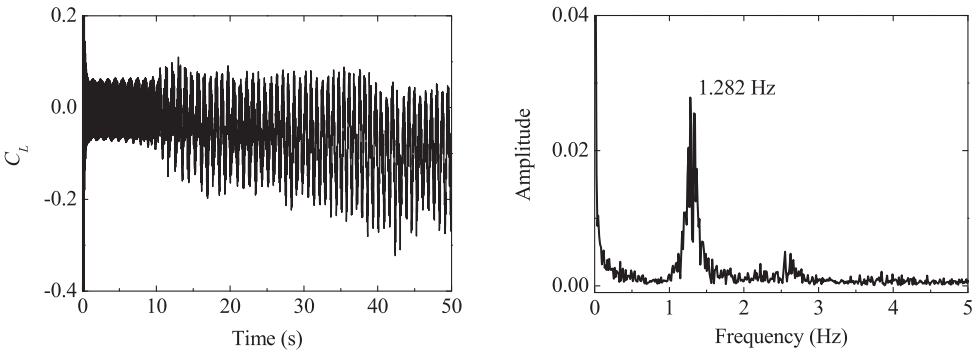

(a) $\theta_0 = 50^\circ$

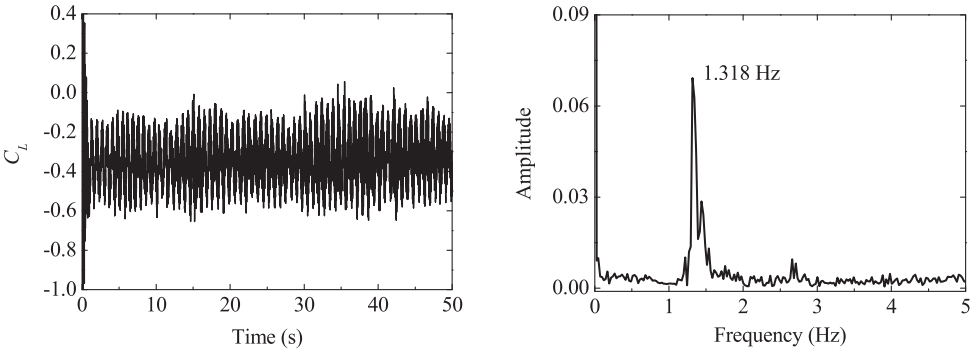

(b) $\theta_0 = 65^\circ$

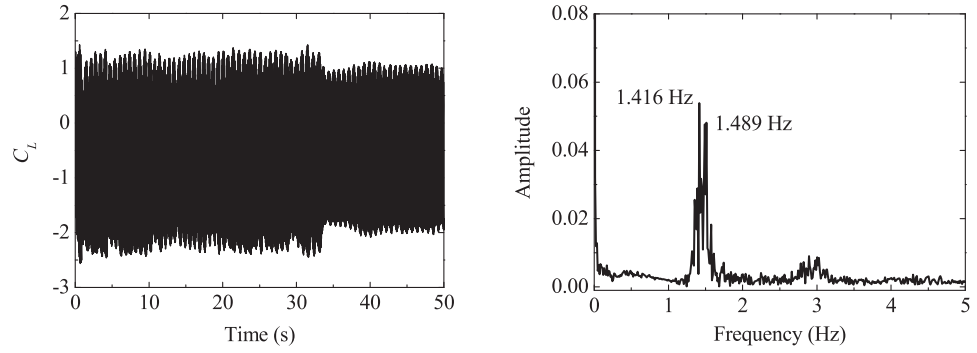

(c) $\theta_0 = 80^\circ$

Fig. 14. Aerodynamic lift coefficients of the CFD cable model with a fixed upper rivulet: (a) $\theta_0 = 50°$; (b) $\theta_0 = 65°$; (c) $\theta_0 = 80°$

J. Bridge Eng., 2013, 18(10): 1021-1031

Oscillating Upper Rivulet" except that the UDF only solves Eq. (2) for the displacement of cable and rivulet, whereas the relative location between cable and the upper rivulet is fixed. The displacement histories of the cable vibration illustrated in Fig. 13 show that no RWIV exists when the upper rivulet is fixed at positions $\theta_0 = 50$, 65, and 80°. Actually, other simulations of the cable with fixed rivulets at different positions of $\theta_0 = 60$ and 70° also give similar results, and the amplitudes of the vibrations are much smaller than the RWIV observed in the wind tunnel tests and described in "One Degree-of-Freedom Cable Model with an Oscillating Upper Rivulet".

The time histories and spectra of aerodynamic lift coefficients at the fixed position angles of 50, 65, and 80° are analyzed and shown in Figs. 14(a–c), respectively. The lift coefficients do not represent the natural frequency of the cable for all cases and hence cannot induce the RWIV of the cable.

Discussion

In the present 2D CFD simulations, RWIV is successfully reproduced by using a preprogrammed oscillating rivulet based on the observation from the wind tunnel test. This verifies the proposed vibrating mechanism and the aerodynamic influence of the upper rivulet on cable vibration. However, the rivulet oscillation and cable vibration are closely coupled, and the behavior of the upper rivulet is also affected by the airflow around it. To understand the whole story of RWIV, a model capable of describing the coupled motion of both the cable and the rivulet should be studied. Moreover, a further investigation using a 3D CFD model will also be necessary.

Different from what previous research indicated, the cable with a fixed upper rivulet does not experience vibration with a large amplitude in the present CFD simulations. The size of the upper rivulet may relate to the issue. As previously mentioned, the relative heights of the rivulet used in the previous experiments are larger than those used in the CFD simulations and, furthermore, are much greater than the measurement results of the wind tunnel experiments. Further study using rivulets of similar size to the measurement results is recommended. In addition, 3D effects of the rivulet, such as axial vortex shedding, are ignored in the 2D simulations of the current study, which might also have effect on the simulation results as well.

According to the results of the wind tunnel test and the CFD numerical simulation described previously, the dynamic properties (amplitude and frequency) and position (equilibrium angle) of the upper rivulet are two essential conditions for RWIV. The results suggest that the existence of the upper rivulet is not sufficient to excite RWIV. To excite RWIV, the upper rivulet should not only oscillate but also oscillate in a certain region with the same frequency as the cable vibration. Because the aerodynamic lift force is the only force acting on the cable being taken into consideration in the CFD simulations, it is believed that the aerodynamic force of the cable would change dramatically and periodically while the upper rivulet oscillates in that special region, introducing negative aerodynamic damping to the system.

Conclusions

In the present paper, an experimental study with UTTMS and CFD simulations are combined to investigate the role the upper rivulet plays in RWIV. The comprehensive study presented in this paper draws the following conclusions:

1. The dynamic properties and position of rivulet obtained by the wind tunnel tests indicated that the rivulet positions will only appear to a specific region with the largest oscillation amplitude and same frequency with the cable vibration when the RWIV occurs; and
2. The CFD simulations of a one degree-of-freedom cable with an upper rivulet fixed on various positions are not able to reproduce the RWIV phenomenon. This suggests that RWIV would not occur if an upper rivulet is present but does not oscillate. The CFD simulation of a one degree-of-freedom cable with a harmonically oscillating upper rivulet reproduces the RWIV phenomenon only when the upper rivulet oscillates between 55 and 75° (with the equilibrium angle of 65°), which agrees well with the wind tunnel test results. This indicates that even if the upper rivulet oscillates on the cable surface, it must oscillate in a certain range to excite RWIV.

Acknowledgments

This research was funded by the National Natural Sciences Foundation of China (NSFC) (90815022, 51161120359, and 51008093). The authors acknowledge Prof. Yaojun Ge, Dr. Lin Zhao, and the staff of the Wind Tunnel Laboratory of Tongji University of China for assistance with this test.

References

ANSYS Fluent 12.1 [Computer software]. Canonsburg, PA, Ansys.

Bosdogianni, A., and Olivari, D. (1996). "Wind- and rain-induced oscillations of cables of stayed bridges." *J. Wind Eng. Ind. Aerodyn.*, 64(2–3), 171–185.

Cosentino, N., Flamand, O., and Ceccoli, C. (2003). "Rain-wind-induced vibration of inclined stay cables. Part I: Experimental investigation and physical explanation." *Wind Struct.*, 6(6), 471–484.

Elmiligui, A., Abdol-Hamid, K. S., Massey, S. J., and Pao, S. P. (2004). "Numerical study of flow past a circular cylinder using RANS, Hybrid RANS/LES and PANS formulations." *Proc., 22nd Applied Aerodynamics Conf. and Exhibit* (AIAA), Providence, RI.

Flamand, O. (1995). "Rain-wind-induced vibration of cables." *J. Wind Eng. Ind. Aerodyn.*, 57(2–3), 353–362.

Gu, M., and Du, X. Q. (2005). "Experimental investigation of rain–wind-induced vibration of cables in cable-stayed bridges and its mitigation." *J. Wind Eng. Ind. Aerodyn.*, 93(1), 79–95.

Gu, M., and Huang, L. (2008). "Theoretical and experimental studies on the aerodynamic instability of a two-dimensional circular cylinder with a moving attachment." *J. Fluids Struct.*, 24(2), 200–211.

Gu, M., and Lu, Q. (2001). "Theoretical analysis of wind–rain induced vibration of cables of cable-stayed bridges." *J. Wind Eng.*, 89, 125–128.

Hikami, Y., and Shiraishi, N. (1988). "Rain-wind-induced vibrations of cables in cable stayed bridges." *J. Wind Eng. Ind. Aerodyn.*, 29(1–3), 409–418.

Li, F. C., Chen, W. L., Li, H., and Zhang, R. (2010a). "An ultrasonic transmission thickness measurement system for study of water rivulets characteristics of stay cables suffering from wind–rain-induced vibration." *Sens. Actuators A Phys.*, 159(1), 12–23.

Li, F. C., and Serizawa, A. (2004). "Experimental study on flow characteristics of a vertically falling film flow of liquid metal NaK in a transverse magnetic field." *Fusion Eng. Des.*, 70(2), 185–199.

Li, H., Chen, W. L., Xu, F., Li, F. C., and Ou, J. P. (2010b). "A numerical and experimental hybrid approach for the investigation of aerodynamic forces on stay cables suffering from rain-wind induced vibration." *J. Fluids Struct.*, 26(7–8), 1195–1215.

Lu, X., Dalton, C., and Zhang, J. (1997). "Application of large eddy simulation to flow past a circular cylinder." *J. Offshore Mech. Arctic Eng.*, 119(4), 219–225.

Main, J. A., and Jones, N. P. (1999). "Full-scale measurements of stay cable vibration." *Proc., 10th Int. Conf. on Wind Engineering: Wind Engineering into the 21st Century,* Balkema, Copenhagen, Denmark, 963–970.

Matsumoto, M., et al. (1990). "Aerodynamic behavior of inclined circular cylinders-cable aerodynamics." *J. Wind Eng. Ind. Aerodyn.*, 33(1–2), 63–72.
Matsumoto, M., Daito, Y., Kanamura, T., Shigemura, Y., Sakuma, S., and Ishizaki, H. (1998). "Wind-induced vibration of cables of cable-stayed bridges." *J. Wind Eng. Ind. Aerodyn.*, 74–76, 1015–1027.
Matsumoto, M., Saitoh, T., Kitazawa, M., Shirato, H., and Nishizaki, T. (1995). "Response characteristics of rain-wind-induced vibration of stay-cables of cable-stayed bridges." *J. Wind Eng. Ind. Aerodyn.*, 57(2–3), 323–333.
Matsumoto, M., Shirashi, N., and Shirato, H. (1992). "Rain-wind-induced vibration of cables of cable-stayed bridges." *J. Wind Eng. Ind. Aerodyn.*, 43(1–3), 2011–2022.
Matsumoto, M., Shirato, H., Yagi, T., Goto, M., Sakai, S., and Ohya, J. (2003a). "Field observation of the full-scale wind-induced cable vibration." *J. Wind Eng. Ind. Aerodyn.*, 91(1–2), 13–26.
Matsumoto, M., Yagi, T., Goto, M., and Sakai, S. (2003b). "Rain-wind-induced vibration of inclined cables at limited high reduced wind velocity region." *J. Wind Eng. Ind. Aerodyn.*, 91(1–2), 1–12.
Matsumoto, M., Yagi, T., Shigemura, Y., and Tsushima, D. (2001). "Vortex-induced cable vibration of cable-stayed bridges at high reduced wind velocity." *J. Wind Eng. Ind. Aerodyn.*, 89(7–8), 633–647.
Ni, Y. Q., Wang, X. Y., Chen, Z. Q., and Ko, J. M. (2007). "Field observations of rain-wind-induced cable vibration in cable-stayed Dongting Lake Bridge." *J. Wind Eng. Ind. Aerodyn.*, 95(5), 303–328.
Peil, U., and Nahrath, N. (2003). "Modeling of rain-wind induced vibrations." *Wind Struct.*, 6(1), 41–52.
Persoon, A. J., and Noorlander, K. (1999). "Full scale measurements on the Erasmus Bridge after rain/wind induced cable vibration." *Natl. Aerosp. Lab. NLR, NLR-TP*, 99063, 1–16.
Phelan, R. S., Sarka, P. P., and Mehta, K. C. (2006). "Full-scale measurements to investigate rain–wind induced cable-stay vibration and its mitigation." *J. Bridge Eng.*, 11(3), 293–304.
Seidel, C., and Dinkler, D. (2006). "Rain–wind induced vibrations–phenomenology, mechanical modelling and numerical analysis." *Comp. Struct.*, 84(24–25), 1584–1595.
van der Burgh, A. H. P., Hartono, and Abramian, A. K. (2006). "A new model for the study of rain-wind-induced vibrations of a simple oscillator." *Int. J. Non-linear Mech.*, 41(3), 345–358.
Verwiebe, C., and Ruscheweyh, H. (1998). "Recent research results concerning the exciting mechanisms of rain-wind-induced vibrations." *J. Wind Eng. Ind. Aerodyn.*, 74–76, 1005–1013.
Wilde, K., and Witkowski, W. (2003). "Simple model of rain-wind induced vibrations of stayed cables." *J. Wind Eng. Ind. Aerodyn.*, 91(7), 873–891.
Xu, Y. L., and Wang, L. Y. (2003). "Analytical study of wind-rain induced cable vibration: SDOF model." *J. Wind Eng. Ind. Aerodyn.*, 91(1–2), 27–40.
Yamaguchi, H. (1990). "Analytical study on growth mechanism of rain vibration of cables." *J. Wind Eng. Ind. Aerodyn.*, 33(1–2), 73–80.
Zuo, D., and Jones, J. P. (2010). "Interpretation of field observations of wind- and rain-wind-induced stay cable vibrations." *J. Wind Eng. Ind. Aerodyn.*, 98(2), 73–87.
Zuo, D., Jones, J. P., and Main, J. A. (2008). "Field observation of vortex- and rain-wind-induced stay-cable vibrations in a three-dimensional environment." *J. Wind Eng. Ind. Aerodyn.*, 96(6–7), 1124–1133.